Spectroscopic evidence of spinel phase clustering in solid solutions $Hg_{1-x}Cr_xSe$ ($0.03 \leq x \leq 0.1$)

2009 J. Phys.: Condens. Matter 21 045603

(http://iopscience.iop.org/0953-8984/21/4/045603)

J. Phys.: Condens. Matter **21** (2009) 045603 (9pp) doi:10.1088/0953-8984/21/4/045603

Spectroscopic evidence of spinel phase clustering in solid solutions $Hg_{1-x}Cr_xSe$ ($0.03 \leqslant x \leqslant 0.1$)

K Lamonova[1], I Ivanchenko[2], S Orel[1], S Paranchich[3], V Tkach[4], E Zhitlukhina[1], N Popenko[2] and Yu Pashkevich[1]

[1] A A Galkin Donetsk Institute for Physics and Engineering of NASU, 83114, Donetsk, Ukraine
[2] Usikov Institute for Radiophysics and Electronics of NASU, 61085, Kharkov, Ukraine
[3] Chernivtsi National University, 58012, Chernivtsi, Ukraine
[4] V N Bakul Institute for Superhard Materials of NASU, 04074, Kyiv, Ukraine

E-mail: lamonova@kinetic.ac.donetsk.ua

Received 27 June 2008, in final form 27 November 2008
Published 8 January 2009
Online at stacks.iop.org/JPhysCM/21/045603

Abstract

The diluted magnetic semiconductors $Hg_{1-x}Cr_xSe$ ($0.03 \leqslant x \leqslant 0.1$) were prepared by the *solid state recrystallization method.* The structure microanalysis of the $Hg_{1-x}Cr_xSe$ compounds, performed by using a scanning electron spectrometer, has shown that the $HgCr_2Se_4$ spinel-like inclusions are present in the host matrix $Hg_{1-x}Cr_xSe$ and their amount increases when the chromium content grows. ESR studies of $Hg_{1-x}Cr_xSe$ samples were carried out in the temperature range 4.2–300 K. ESR spectra of the samples with different chromium contents demonstrate the same g-factors at room temperature and similar fine structure development with the temperature decrease. Numerical studies of g-factors, performed by the modified crystal field approach (MCFA), allowed us to reveal that Cr^{2+}/Cr^{3+} ions in the tetrahedral environment of the solid solution $Hg_{1-x}Cr_xSe$ cannot lead to the ESR signal. The experimental g-factor is well reproduced by a numerical g-factor for Cr^{3+} ions located in the octahedral environment, being specific for the $HgCr_2Se_4$ spinel phase. The onset of the ESR fine structure is determined by the trigonal distortions of the $(CrSe_6)^{9-}$ octahedral cell. From our study it has been found that the spinel clusters are present in the $Hg_{1-x}Cr_xSe$ solid solution even at low chromium content.

(Some figures in this article are in colour only in the electronic version)

1. Introduction

Diluted magnetic semiconductors (DMSs) are compounds with structures like $A_{II}B_{VI}$ ([Zn, Cd, Hg]: Se or [Zn, Cd, Hg,]: Te) and $A_{III}B_V$ ([Al, Ga, In]: As or [Al, Ga, In]: N), which contain a controllable number of magnetic ions randomly distributed over the host matrix. The transition elements (Cr, Mn, Fe, Co) or the rare earth ions (Eu, Gd, Er) can serve as the magnetic inclusions [1]. Such semiconductor alloys contain two interacting electron subsystems: the delocalized band of s, p electrons, which originate from the non-magnetic host semiconductor, and the localized d electrons, associated with the magnetic ions [2]. Consequently, the magnetic properties of these materials depend on the coupling between spins of the band carriers and localized spins of the magnetic ion electrons, resulting in the enhanced magneto-optical and magneto-electronic responses. In addition, it gives a chance to control magnetization as well as magneto-transport properties of the DMS materials by the electric field [3].

The coupling between the dopant-induced magnetic ions can result in appearance of different magnetic orderings (spin glass and anti-and ferromagnetic phases). Therefore, the magnetic order formation will depend on three factors: (i) on the nature of the host semiconductor, (ii) on the physical and chemical characteristics of the magnetic dopant, (iii) on the technology process of crystal growth. The

magnetic order formation can be accompanied by material decay into nanoscale metallic ferromagnetic clusters within a semiconductor lattice. Such clustering gives rise to the creation of new phase structure with a symmetry that differs from the host lattice symmetry [4]. As a result, the mismatched crystal lattices coexist in the bulk of the crystal and a strain on the boundaries can lead to structure instability [5, 6]. As regards the practical usefulness of DMSs, these materials seem to be very attractive as the sources of spin-polarized current in spintronic devices [8–10]. In this respect, one of the requirements for the DMSs is that the Curie temperature should be as close as possible to room temperature or higher [11, 12].

The mercury (II) selenide ($Hg_{1-x}Cr_xSe$) is a chemical compound with a host sphalerite structure HgSe, doped by chromium ions, which is a convenient model for studying the effects connected with the space charge ordering in the impurity systems with a mixed valence. Such materials are characterized by the presence of a resonance n-type level being located deeply in the valence band and, as a result, the chromium concentration is stabilized. The Coulomb repulsion between the impurity ions results in their space correlation. Because the space correlated charged admixtures diffuse the electrons less than disordered charged centers, the electron mobility increases in an anomalous way. The last feature seems to be a highly promising one for designing spin-polarized transport based devices.

The results of measuring the electron mobility and the chromium ion concentration (x) in the $Hg_{1-x}Cr_xSe$ ($0.03 \leqslant x \leqslant 0.1$) crystals [13] show that the chromium ions can be in at least two different charge states (Cr^{2+}, Cr^{3+}), being distributed over the crystal non-uniformly because of the bad chromium solubility in HgSe. Based on the ESR spectra and magnetic susceptibility studies of the $Hg_{1-x}Cr_xSe$ ($0.00112 < x < 0.07$) samples, prepared by the modified Bridgman's method, the authors established the fact of transition to the spin glass phase [14], which is accompanied by low-symmetric lattice distortions originating due to heating. The authors noticed a temperature of these distorted insertions as well as a rise of the phase transition temperature with the chromium content increase. In fact, the diamagnetic matrix HgSe is a face centered cubic (FCC) lattice with the $T_d^2(F\bar{4}3m)$ symmetry group. The degree of HgSe packing is rather low and amounts to $f = 0.62$. Under replacement of the Hg^{2+} ions by the chromium ions (Cr^{2+}, Cr^{3+}) the packing index decreases by 8% and 13%, respectively. This originates from a difference between the radii of Hg^{2+} and chromium ions. A similar packing index decrease leads inevitably to crystal structure distortion so that the number of cavities becomes minimal in the sample. In this case, one may expect a lattice constant decrease. The dependence of the lattice parameter on the chromium content in $Hg_{1-x}Cr_xSe$ [15] shows that with a chromium ion increase the lattice parameter decreases and at $x = 0.05$ it reaches the minimal value. More detailed investigations of the $Hg_{1-x}Cr_xSe$ magnetic properties allowed the authors to conclude that the $Hg_{1-x}Cr_xSe$ compound is homogeneous for $x < 0.05$. The chromium concentration increase leads to the crystal structure transformation. As a consequence, new crystal ferromagnetic inclusions like CrSe and $HgCr_2Se_4$ arise.

Below we shall focus on (a) the investigations of ESR spectra of the $Hg_{1-x}Cr_xSe$ ($0.03 \leqslant x \leqslant 0.1$) crystals grown by the *solid state recrystallization method*, which in contrast to the Bridgman's method allows obtaining a more homogeneous distribution of the Hg, Cr, and Se components; (b) the study of electron spectra of the Cr^{2+} and Cr^{3+} ions in the $Hg_{1-x}Cr_xSe$ and $HgCr_2Se_4$ compounds by the modified crystal field approach (MCFA); (c) the identification of the type of structure and its possible distortions by means of the g_{calc}-factor calculation and its comparison with the g_{exp}-factor obtained from the experimental ESR spectra.

2. Samples and technology

The ingots of $Hg_{1-x}Cr_xSe$ with the initial chromium content $0.03 \leqslant x \leqslant 0.1$ were grown by the solid state recrystallization method. By taking into account that the state diagram of the solid solutions $Hg_{1-x}Cr_xSe$ is unknown, both the synthesis temperature and the crystal growth temperature were chosen in an experimental way. For example, the synthesis temperature was equal to 850 °C and 860 °C for compositions $x = 0.03$ and 0.05, respectively. The substance synthesis was carried out in the oscillating stove in the quartz ampoules covered by pyrolytic carbon because of possible ampoule explosion under the high pressure of the mercury vapor. The synthesis conditions were as follows: (i) up to the temperatures $T = 350$–400 °C a rise of temperature was realized with a 100° C h^{-1} rate; (ii) at $T > 400$ °C the temperature was raised with a 20–30° C h^{-1} rate up to the fusion temperature $T = 850$–860 °C. After curing at this temperature for 18–24 h the stove was cooled along with the ampoule to room temperature, keeping the ampoule upright. The crystal growth was carried out at the temperature gradient on the solid–melt interface $T \sim 110$ °C with a 0.35 mm h^{-1} rate. During the growth process the substance loaded ampoule was rotated with a 2 turn/min rate. Since in the process of crystal growth the segregation coefficient is unequal to unity and consequently the impurity distribution along the ingot is non-uniform, the analysis of characteristics of the solid solution $Hg_{1-x}Cr_xSe$ with such chromium content has been carried out for the samples cut off from the middle part of the ingots.

We have carried out the microanalysis of the sample content on the scanning electron microscope ZEISS EVO 50XVP with a combined system of the energy-dispersion analysis INCA ENERGY 450 and structural HKL Channel 5 analysis. It was found that all samples under test have non-homogeneous composition irrespective of the initial chromium content: for any sample area we could observe dark colored impurities on the light tone of the basic matrix. As an example, the analyzed surface part of the sample with the initial chromium content $x = 0.05$ is shown in figure 1 in the characteristic x-ray emission of C_K, Cr_K, Se_L, and Hg_M elements. We used the operating mode of the spectrometer so that the analyzed surface area of the sample was less than 1 μm. This was quite enough to distinguish all lines of the elements under test and to exclude a possible influence of surroundings on the microanalysis data. The detailed analysis of the sample composition performed for some typical areas

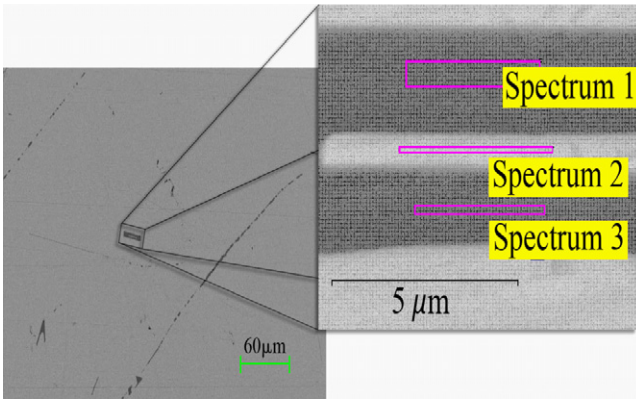

Figure 1. Surface imaging of the sample $Hg_{1-x}Cr_xSe$ with the initial chromium content $x = 0.05$ in the characteristic x-ray emission of C_K, Cr_K, Se_L, and Hg_M elements: the surface of the whole sample (left) and the surface of part of the sample (right).

Table 1. The sample composition. (Note: all results are presented in weight percentages.)

Spectrum	C	Cr	Se	Hg	Total
1	3.05	15.44	46.64	34.86	100.00
2	4.41	4.03	31.51	60.04	100.00
3	3.56	14.73	45.81	35.90	100.00

shows that a percentage of Hg, Cr, and Se elements on the dark areas corresponds to that characteristic for the spinel phase $HgCr_2Se_4$ (table 1, spectra 1, 3). In this case, the light areas on the electron-diffraction patterns correspond to the solid solution $Hg_{1-x}Cr_xSe$ (table 1, spectrum 2). By taking into account the valence of elements that are part of the probe, one may convert easily the weight percentages to atomic ones without sensitivity losses. The carbon availability in the samples is most probably caused by utilizing in the technological process of the crystal growth the pyroelectric carbon covering the cuvette's walls. However, we did not carry out the direct investigations of the carbon occurrence in the sample during the growth process. Thus, at least two different phases are in the samples under test, namely the $Hg_{1-x}Cr_xSe$ phase and the $HgCr_2Se_4$-like phase. At the same time, unlike the samples grown by Bridgman's method and described earlier in the paper [15], the inclusions of the CrSe phase are absent here.

3. Analysis of $Hg_{1-x}Cr_xSe$ electron spectra by the ESR method

Spectroscopic investigations of diluted magnetic semiconductors $Hg_{1-x}Cr_xSe$ were carried out in the temperature range 4.2–300 K on the ESR spectrometers at the frequencies $f_1 = 9.7173$ GHz and $f_2 = 34.163\,99$ GHz (ELEXYS E580 Super Q-FT).

First, it is worth noting that for the samples with different chromium contents the ESR spectra at room temperature are asymmetric single lines with the same g-factor values (table 2), whereas the width of the ESR line increases by about 20% with the chromium content increase from $x = 0.03$ to 0.10.

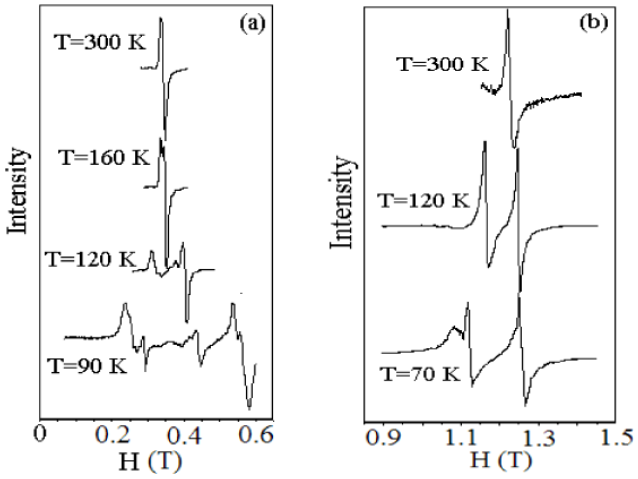

Figure 2. ESR spectrum development of $Hg_{0.95}Cr_{0.05}Se$ with the temperature decrease: (a) $f_1 = 9.7173$ GHz; (b) $f_2 = 34.163\,99$ GHz.

Table 2. Experimental g-factor values, measured at the room temperature.

Content	g-factor	ΔH (mT)
0.03	1.9831	9.4
0.05	1.9850	10.0
0.07	1.9838	11.6
0.10	1.9841	12.0

It has been found experimentally that the temperature dependence of the ESR spectra remains virtually the same for all samples under test. Because of this, we carry out the analysis of experimental data in detail for the solid solution $Hg_{1-x}Cr_xSe$ with the initial chromium content $x = 0.05$ (figure 2). The ESR spectrum measurements at the frequency $f_1 = 9.7173$ GHz show that with a temperature decrease the single and slightly asymmetrical ESR line becomes a non-homogeneously broadened one and at the temperatures $T < 120$ K it splits into two non-homogeneously broadened ESR lines (figure 2(a)). From ESR spectra (figure 2(b), $f_2 = 34.163\,99$ GHz), it has been found that at the temperature $T = 120$ K the right ESR line (see figure 2(a)) consists of two resonance lines with equal widths ($\Delta H_L = 7.9$ mT and $\Delta H_R = 8.2$ mT, respectively) (see figure 2(b)), which are narrower than that at room temperature ($\Delta H = 14.9$ mT), pointing out an increase of the exchange interaction. A situation like this can appear when the $HgCr_2Se_4$ impurities transfer into the ferromagnetic phase. It is worth also noting that the temperature decrease to $T = 70$ K leads to a splitting of the left ESR line and broadening of the right ESR line ($\Delta H_R = 15.6$ mT) (figure 2(b)).

Thus, starting with a temperature $T = 120$ K and below, ESR spectra possess fine structure. This can be interpreted as an interaction of the chromium ion levels, which are non-equidistantly split by the magnetic field. The aforementioned temperature behavior of the ESR spectra may be evidence of increasing the local magnetic fields produced by the adjacent spins under transition of spinel $HgCr_2Se_4$ inclusions in the

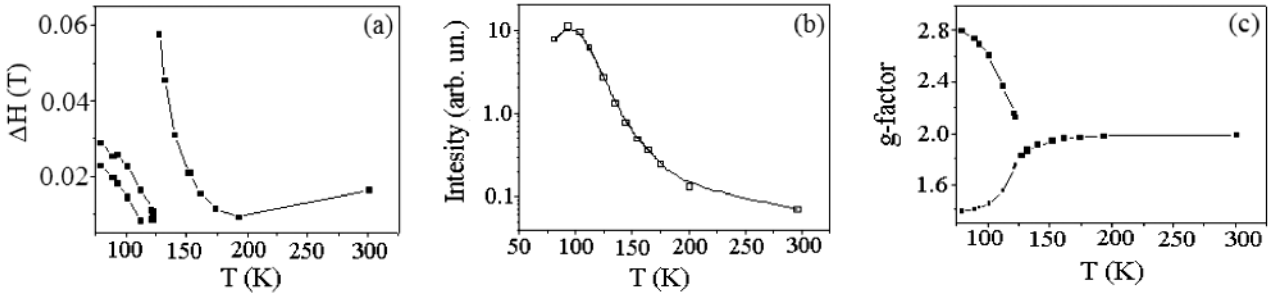

Figure 3. Temperature dependences of the ESR spectrum parameters for the sample with $x = 0.03$ at the frequency $f_1 = 9.7173$ GHz: (a) ESR line width; (b) integral intensity of the whole ESR spectra; (c) g-factor. In all figures, the lines are a guide to the eye.

ferromagnetic phase. Interestingly, a similar ESR fine structure is observed in ESR spectra of the pure $CdCr_2Se_4$ compound around the Curie temperature [16].

The temperature dependences of ESR spectra parameters confirm all facts noted above (see figure 3). At the frequency $f_1 = 9.7173$ GHz and temperatures $T < 120$ K, we observe a change in the left and right ESR line widths (figure 3(a)). A Curie–Weiss law with the temperature $\theta = 121$ K approximates the temperature dependence of the ESR line intensity (figure 3(b)). This is inherent to the $HgCr_2Se_4$ ferromagnetic spinel with $T_C = 106$ K [17]. Moreover, the g-factor remains constant ($g \approx 1.98$) with the temperature decrease up to 120 K (figure 3(c)) just as observed for some ferromagnetic spinels in [18, 19]. The aforementioned changes in the experimental ESR spectra are the same for all samples with different chromium contents.

In spite of many similarities in behavior of the ESR spectra of the $Hg_{1-x}Cr_xSe$ and the spinel $HgCr_2Se_4$, we are not sure that the Cr^{2+} or Cr^{3+} ions in the tetrahedral coordination of the $Hg_{1-x}Cr_xSe$ solid solution could contribute to the ESR signal. In order to define the origin of the spin resonance and the fine structure, the calculations of Cr^{2+} and Cr^{3+} electron spectra as well as the g-factors both in the tetrahedral (for the $Hg_{1-x}Cr_xSe$) and octahedral (for the $HgCr_2Se_4$) environment should be carried out.

4. Electron spectrum calculations and discussion

The divalent chromium ion (Cr^{2+}:$3d^4$) has three different spin states: the high spin state ($S = 2$), the intermediate spin state ($S = 1$) and the low spin state ($S = 0$). The 25-fold degenerate high spin term ^5D is the ground state, which is in accordance with Hund's rules. The trivalent chromium (Cr^{3+}:$3d^3$) has two spin states, namely high ($S = 3/2$) and low ($S = 1/2$) spin states. In this case the ground state is the ^4F high spin term [20, 21].

For the g-factor calculations we used the modified crystal field approach [22, 23] in which we added standard Zeeman's term

$$V_H = \mu_B \sum_{i=1}^{n} (\vec{l}_i + 2\vec{s}_i, \vec{H}),$$

where μ_B is the Bohr magneton, operators $\vec{l}_i$ and $\vec{s}_i$ are the orbital and spin moments for the ith electron, and $\vec{H}$ is a magnetic field. We operate with a full orthonormalized system of the multi-electron functions of the atomic Hamiltonian: $\Psi(\gamma\ SLM_SM_L;\ 3d^n)$ with $n = 3$ and 4 for Cr^{2+} and Cr^{3+}, respectively. These functions, in turn, are linear combinations of the *multi-electron determinant functions* Φ, (1, 2, 3) and Φ (1, 2, 3, 4) (the numbers correspond to the one-electron wavefunctions $\psi_i(nlm_lm_s)$ for each of the 3d electrons). In the case of the one-electron wavefunctions, we operate with the hydrogen-like wavefunctions which contain the parameter $\alpha = Z_{\text{eff}}/n\,a_B$. Here, n is the principal quantum number, a_B is the Bohr's radius and Z_{eff} is the effective nuclear charge for the given metallic ion. This value attributes a difference between the nuclear charge and screening constant and is calculated by Slater's rules [24]. For the free ion the screening constant and, hence, the Z_{eff} value depend on the inner electrons only. However, for the ion, which is included in some crystal environment, the Z_{eff} magnitude decreases because of an additional screening which arises due to the ligand's electron density. In this case, there is a need to use the corrected value $Z'_{\text{eff}} = Z_{\text{eff}} - \Delta Z_{\text{eff}}$ for the one-electron wavefunctions. The magnitude of ΔZ_{eff} depends on the ion oxidation number as well as on the kind and the number of ligands, and it varies within the range of 10–15% for the divalent ions and 15–20% for the trivalent ions [23] approximately. Thus, the Z_{eff} change allows calculating the covalence degree implicitly. Therefore, in contrast to the traditional crystal field theory [25, 26], the crystal field problem can be parametrized in a new fashion that gives a possibility to calculate the coordination complexes with different symmetries and various ligand surroundings. Moreover, the spin–orbit bond constant and, therefore, the g-factor are functions of the effective nuclear charge. By taking into account the external magnetic field effect upon the ion spectrum, we can calculate the g-factor numerically without using the spin-Hamiltonian approach.

4.1. The study of electron spectra for Cr^{2+} ions in the undistorted tetrahedral crystal field

Let us consider the Cr^{2+} ion placed in the center of an undistorted tetrahedral coordination complex $(CrSe_4)^{6-}$ of the four Se^{2-} ions, which are located at the corners of a cube with the side $a/2$ ($a = 6.0837$ Å at $x = 0.03$ [15]). The distances of Cr–Se are identical and equal to 2.63 Å, i.e. equal to Hg–Se distances in the HgSe sphalerite structure.

The calculation of electron spectra for Cr^{2+} ions without taking into account both the spin–orbit interaction and the

magnetic field results in the high spin ($S = 2$)–low spin ($S = 1$) transition at the point $Z_{\text{eff}} = 4.0$. Because this value is much less than $Z_{\text{eff}} = 4.95$ for the free Cr^{2+} ion, estimated by the Slater's rules, such a transition can be realized under some special conditions (for instance, either high pressures or high temperatures).

To calculate the electron spectrum including the spin–orbit coupling between 3d electrons, we choose the model potential in the following form:

$$\hat{V}_{\text{SO}} = \sum_{i=1}^{6} \xi(r_i)(\hat{l}_i, \hat{s}_i).$$

Here, $\xi(r_i)$ is a one-electron constant of the spin–orbit interaction—$\xi(r_i) = -\frac{e\hbar^2}{2m^2c^2}\frac{1}{r_i}\frac{\partial U(r_i)}{\partial r_i}$, where $U(r_i)$ is a field potential in which the electron moves. The form of a one-electron potential can be chosen under the assumption that a computed spin–orbit constant ξ_{3d} should coincide, within a reasonable accuracy, with an experimental one. For instance, as to the chromium ion: $\xi_{3d}^{(Cr^{2+})} \approx 230$–$256\ \text{cm}^{-1}$ [21, 27–29] and $\xi_{3d}^{(Cr^{3+})} \approx 275$–$296$ [21, 29]. Thus, the deduced form of such a potential yields

$$\xi_{nl} = \frac{\alpha^2}{2}\frac{Z^{2+\delta}Z_{\text{eff}}^2}{n^3 l(l+1)(l+1/2)}(\text{a.u.}),$$

where $\alpha = e^2/\hbar c$ is the fine structure constant, n is a principal quantum number, l is an orbital quantum number and Z is a nuclear charge, $\delta = 0.05$ for the Cr^{2+} ion and $\delta = 0.06$ for the Cr^{3+} one.

Taking into account the spin–orbit interaction between d electrons for the Cr^{2+} results in the splitting of the ground crystal term $^5T_2$ into four spin triplets, a spin doublet and a non-magnetic spin singlet, which is the ground one. The external magnetic field splits the two- and threefold degenerate levels, but a singlet remains invariable. The total splitting of the basic $^5T_2$ level is more than $300\ \text{cm}^{-1}$. Hence, it is possible to suppose that in the temperature range (70–300) K the levels are occupied up to $200\ \text{cm}^{-1}$ and one should consider all the allowed transitions in this range. Namely, it is necessary to look at $2 \leftrightarrow 3, 3 \leftrightarrow 4$ transitions and $5 \leftrightarrow 6, 6 \leftrightarrow 7$ ones, whereas $2 \leftrightarrow 4, 5 \leftrightarrow 7$ and $8 \leftrightarrow 9$ transitions are forbidden (see the inset in figure 4). One can see that none of the transitions gives the experimentally observable value of the g-factor ($g_{\text{exp}} \sim 1.98$) in the whole range of the effective nuclear charge changing.

Due to all of this we conclude that the ESR signal, which is registered at the temperatures $T < 300$ K, does not originate from the Cr^{2+} in the undistorted tetrahedral surrounding.

4.2. Effect of the tetrahedral distortions on the $Hg_{1-x}Cr_xSe$ ESR spectrum

The low-symmetry crystal field induced by the tetrahedron deformations results in additional orbital splitting; namely, the lattice distortions like Q_2 and Q_3, which transform over two-dimensional E representation, split the $^5T_2$ level into the orbital doublet and basic singlet. The tetrahedron distortions, which transform over three-dimensional F_2 and F_1 representations,

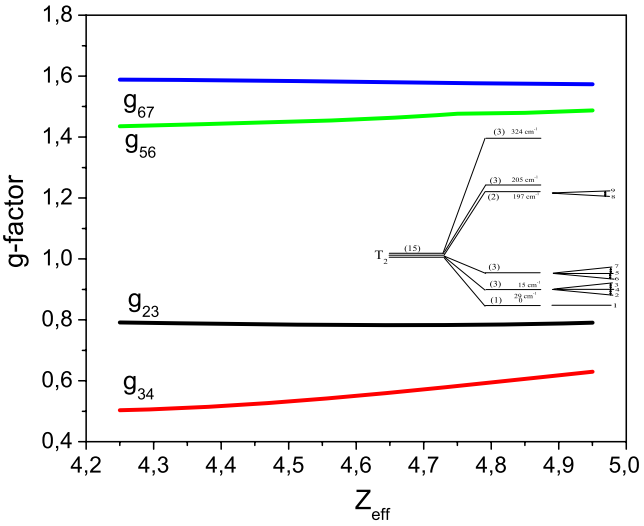

Figure 4. The dependence of g-factor values for the allowed transitions of the $(CrSe_4)^{6-}$ undistorted tetrahedral complex on the Z_{eff}. The inset shows the Cr^{2+} level-splitting schemes, calculated for $Z_{\text{eff}} = 4.95$.

remove the orbital degeneration completely with the exception of the Q_9 distortion, which acts like the Q_3 one [30]. The spin–orbit interaction lifts the remaining spin degeneracy so that the five- and tenfold degenerated levels split into the separate singlets and doublets. An external magnetic field results in the final level splitting. It is worth noting that the transitions between split doublet levels are forbidden by the selection rules. The possible transitions between different singlets, which are separated by the so-called zero field splitting value ΔE_{ZFS} (ZFS), should violate the ratio $f_1/f_2 = H_1/H_2$, where the $H_{1,2}$ values are the resonance field magnitudes, while in our experiments the same g-factor values are obtained for two different quanta.

Therefore, the aforementioned calculations allow us to conclude that the Cr^{2+} ion, which is placed in the tetrahedral surroundings, could not be the origin of the ESR signal observed experimentally.

4.3. The study of the electron spectra for Cr^{3+} ions in the undistorted tetrahedral and octahedral crystal fields

Let us consider the tetrahedral $(CrSe_4)^{5-}$ and octahedral $(CrSe_6)^{9-}$ complexes with the trivalent chromium ion Cr^{3+}. We shall suppose that a tetrahedral $(CrSe_4)^{5-}$ complex is arranged similarly to that described in section 4.1. The octahedral $(CrSe_6)^{9-}$ complex is a chromium ion located in the cubic center and six selenium ions located at the centers of the cube sides. The cube side is $a/2$ ($a = 10.7418$ Å) and the distances R(Cr–Se) equal to 2.538 Å, which are characteristic for the $HgCr_2Se_4$ spinel structure [31].

The dependences of the lowest energy levels on Z_{eff} have been calculated for the undistorted tetrahedral and octahedral complexes without taking into account the spin–orbit interaction and magnetic field. Within the range of $4.3 \leqslant Z_{\text{eff}} \leqslant 5.3$ these spectra do not demonstrate spin state transitions between the lowest high ($S = 3/2$) and excited low

($S = 1/2$) spin states. The point $Z_{\text{eff}} = 5.3$ corresponds to the effective nuclear charge for the free Cr^{3+} ion calculated by the Slater rules [24]. Further, we shall consider only the high spin state for the Cr^{3+} ion in both complexes.

The crystal field splits the basic electron term ^4F of the Cr^{3+} ion into the three crystal terms depending on the ligand's symmetry: in the case of tetrahedral T_d symmetry $^4F = {}^4A_1 + {}^4T_2 + {}^4T_1$ while in the case of cubic O_h symmetry $^4F = {}^4A_{2g} + {}^4T_{1g} + {}^4T_{2g}$. For the tetrahedral case the orbital triplet $^4T_1$ is the basic one with the 12-fold degeneracy overall. For the cubic case, the orbital singlet $^4A_{2g}$, which is fourfold degenerated by the spin, is the basic one [21].

Accounting for spin–orbit coupling does not result in the evident splitting of the $^4A_{2g}$ term while the crystal triplet $^4T_2$ splits into the two spin quartets and two spin doublets in such a way that one of the spin quartets is the lowest level. Thus, in both the undistorted tetrahedral and octahedral crystal fields the spin quartet is the ground state. However, the distance up to the nearest excited level in the case of the octahedral crystal field is ten times as much as that in the case of the tetrahedral crystal field (see the insets in figure 5).

An external magnetic field splits the aforementioned spin quartets in a different way. In the case of the octahedral crystal field, the arbitrarily directed magnetic field splits the lowest $^4A_{2g}$ quartet into the four spin singlets, which are equidistant, and the transitions $1 \leftrightarrow 2$ and $2 \leftrightarrow 3$ as well as $3 \leftrightarrow 4$ are allowed (left inset in figure 5).

In the tetrahedral case, the lowest quartet splits into the two quasi-doublets in such a way that the splitting between quasi-doublets is much bigger than those located inside the quasi-doublets. The transition $1 \leftrightarrow 2$ has vanishingly small intensity, i.e. it is forbidden, whereas the transitions $1 \leftrightarrow 3$ and $1 \leftrightarrow 4$ as well as $2 \leftrightarrow 3$ and $2 \leftrightarrow 4$ are allowed (right inset in figure 5). Thus, the ESR signal originates from the transitions between two quasi-doublets and further we shall follow the $1 \leftrightarrow 4$ transition as its main representative. The calculated g-factors are shown in figure 5, where curve 1 corresponds to the octahedral case for the transition $1 \leftrightarrow 2$, and curve 2 corresponds to the tetrahedral case for the transition $1 \leftrightarrow 4$.

As is evident from figure 5, curves 1 and 2 demonstrate different behavior: with the Z_{eff} increase, curve 2 falls down much faster than curve 1, while the g-factor magnitude, calculated for the Cr^{3+} ion embedded into the octahedral selenium cell, varies in the narrow range between 1.9 and 1.98 for a wide change of the effective nuclear charge. The last result correlates quite well with the experimental data presented in [18, 19, 21], where the g-factor varies in the range from 1.97 to 1.99 for the different types of spinels at the temperatures $T > T_C$ and virtually does not depend on the ligand surroundings.

In spite of the fact that the calculated g-factor (curve 2) reaches $g_{\text{exp}} = 1.9831$ around the point $Z_{\text{eff}} = 4.9$, we cannot consider the Cr^{3+} ion, which is placed in the undistorted tetrahedral cell, as the origin of the ESR signal for some reasons. The experimental temperature dependence of the g-factor demonstrates a constant behavior in a wide temperature range (figure 3(c)). This means that neither the structural distortions nor the crystal field modifications, which take place under the temperature changes [15], result in the g-factor variation. Since the effective nuclear charge changing can be interpreted as a crystal field variation, the steep dependence of $g(Z_{\text{eff}})$ contradicts the experimental observations. Another reason for this is the difference between the radii of Hg^{2+} and Cr^{3+} ions, that does not allow us to consider the $(CrSe_4)^{5-}$ complex as the undistorted one.

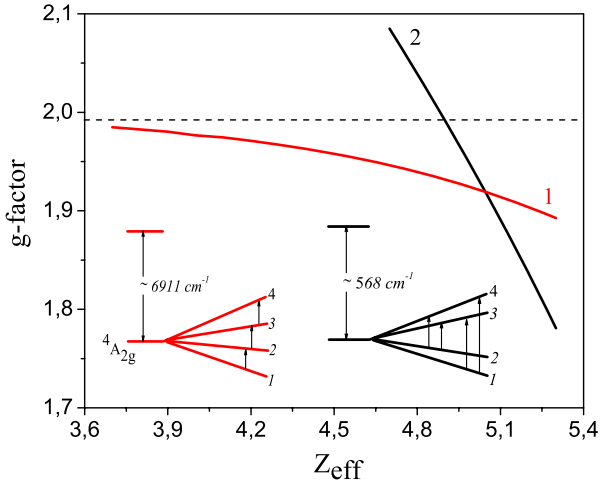

Figure 5. The dependences of g-factor values on Z_{eff} for the Cr^{3+} ion embedded into the crystal octahedral (curve 1) and tetrahedral (curve 2) complexes. The insets show the Cr^{3+} ion level-splitting schemes, calculated for $Z_{\text{eff}} = 5.3$.

Thus, we come to the following conclusions. (a) The Cr^{3+} ion, embedded in the undistorted tetrahedral complex, could not be a reason for the ESR signal at the room temperature. (b) In contrast, the Cr^{3+} ion, placed in the undistorted octahedral cell, could explain the stable ESR signal at room temperature for the chromium content $x \geqslant 0.03$.

4.4. Lattice distortions and their effect on the ESR spectrum features in the $Hg_{1-x}Cr_xSe$

Various crystal deformations caused by the ion's displacements [7, 32] are factors which have an important influence on the ion electronic spectrum. The difference in the radii of the Hg and Cr ions can be a reason for both the Se-cell distortions and off-centering shifts of the Cr ions. Further, we shall learn the most probable distortions of the tetrahedral and octahedral complexes and their effect on the g-factor value. Moreover, a question about the ESR fine structure development with the temperature decrease remains unresolved. We shall check a model of the ESR fine structure appearance and its development due to the trigonal distortions of the $(CrSe_6)^{9-}$ octahedral complex, presented in the real lattice of the $HgCr_2Se_4$ spinel.

From the beginning, let us consider the possible distortions in the $(CrSe_4)^{5-}$ tetrahedron. As mentioned above, the trivalent chromium ion has a smaller radius than the mercury ion $R(Cr^{3+}) = 0.61$ Å, $R(Hg^{2+}) = 0.96$ Å, [33]), hence, the difference in the radii is more than 30%. Thus, the substitution of the mercury by the trivalent chromium in the host tetrahedral matrix provides the additional degree of freedom for off-centered shifting of the chromium ion as well

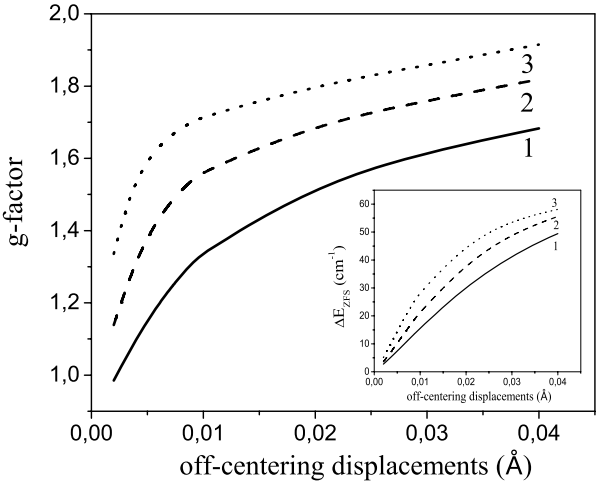

Figure 6. Dependence of the g-factor calculated for the transition $1 \leftrightarrow 2$ at different magnitudes of the effective nuclear charge, on the chromium off-centering removal: $1 - Z_{\text{eff}} = 5.3$; $2 - Z_{\text{eff}} = 5.0$; $3 - Z_{\text{eff}} = 4.7$. Inset: the dependence of the ZFS on the chromium off-centering removal.

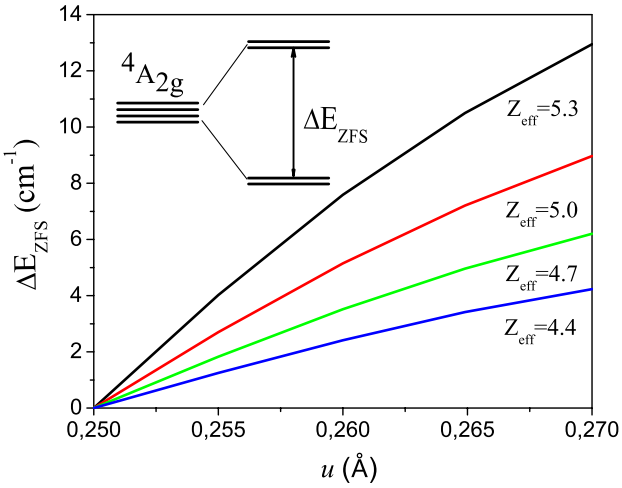

Figure 7. Dependences of the zero field splitting energy ΔE_{ZFS} for the Cr^{3+} ions, placed in the $HgCr_2Se_4$ spinel structure, on the magnitude u.

as for the distortion of the ligand's cell. One may estimate the approximate magnitude of the off-centered shifting. The Cr–Se distance is equal to 2.63 Å in HgSe sphalerite structure, while $R(Cr^{3+}) + R(Se^{2-}) = 2.59$ Å. The difference is equal to 0.04 Å and, therefore, the chromium ion shift towards the one of selenium ions cannot be more than this value. However, such a shifting leads to the symmetry reduction and, as a result, to the splitting of the quartet into the two doublets. The distance between the doublets, the so-called zero field splitting value (ZFS), depends on both the effective nuclear charge and Cr^{3+} shift value (see figure 6). At this, the electron transition $1 \leftrightarrow 2$ becomes an allowed one, while the electron transitions $1 \leftrightarrow 3$ and $1 \leftrightarrow 4$ are forbidden.

It is quite clear that the increase of the crystal field, which appears in the effective nuclear charge decrease and the chromium off-centering shift increase, results in the drastic increase of both the ZFS value and g-factor. Thus, in an effort to reach the experimental value of g-factor sizeable off-centering displacements should be present. Furthermore, the sharp increase of the ΔE_{ZFS} on the chromium displacements does not allow for explanation of the ESR spectrum fine structure.

Nevertheless, one may assume that the $Hg_{1-x}Cr_xSe$ phase, which consists of the strongly distorted $(CrSe_4)^{5-}$ tetrahedral complexes, can originate the ESR signal. If this assumption is right, the ESR signal should be present in the ESR spectrum for any chromium content x, starting with negligibly small ones. This assumption could be checked experimentally.

Finally, we consider the influence of distortions on the octahedral complex $(CrSe_6)^{9-}$. The space group of the $HgCr_2Se_4$ spinel compound is $Fd\bar{3}m$ with the ion coordinates shown in table 3. It is easy to see that chromium ions possess the D_3d site symmetry that the trigonal distorted octahedron naturally adopts. The degree of distortion is characterized by the magnitude of the parameter u. If this parameter is equal to $u_0 = 0.25$, the octahedron is undistorted and the

Table 3. Atomic coordinates for $HgCr_2Se_4$ [27].

Atom	Ox.	Wyck.	Symm.	x	y	z
Hg	+2	8a	$\bar{4}3m$	1/8	1/8	1/8
Cr	+3	16d	$\bar{3}m$	1/2	1/2	1/2
Se	−2	32e	$3m$	u	u	u

Cr^{3+} ground state is $^4A_{2g}$ (see the inset in figure 7). Trigonal distortions lead to the $^4A_{2g}$ term splitting into the two spin doublets, with the energy splitting ΔE_{ZFS} depending on the u-value. For instance, for the parent compound $HgCr_2Se_4$ at room temperature the parameter u is equal to 0.2649 [27]. Furthermore, in [34] the author asserts that the trigonal distortions accrue (u-value increases) with the temperature decrease.

An increase of the u-value results in a linear decrease of the octahedral volume, i.e. an increase of the crystal field strength. Note that a change of the u-value does not provoke a change in the primitive cell volume. Thus, the ΔE_{ZFS} value increases if the u-value increases at the given effective nuclear charge, and the ΔE_{ZFS} value decreases with the Z_{eff} value decrease (figure 7). In contrast to the off-centering in the tetrahedral complex, the ΔE_{ZFS} alterations in the octahedral complex occur in the scale of ten wavenumbers.

In the trigonal distorted octahedral complex $(CrSe_6)^{9-}$ the ESR spectrum becomes drastically anisotropic. Both the structure anisotropy and the splitting into the two quasi-doublets can explain the development of the ESR spectrum fine structure. In order to illustrate this, we calculate the frequency field dependences in a distorted octahedron with $u = 0.255$ for the three different orientations of magnetic field (figure 8). Actually, there is no way to determine the real orientation of the $HgCr_2Se_4$ spinel clusters in the host matrix HgSe; however, we can expect that this orientation is not chaotic.

Experimental values of g-factors can be achieved by the small trigonal distortions deviating about 0.5% from the undistorted case $u_0 = 0.25$. In figure 9 we show the g-factor dependences on the effective nuclear charge for the low

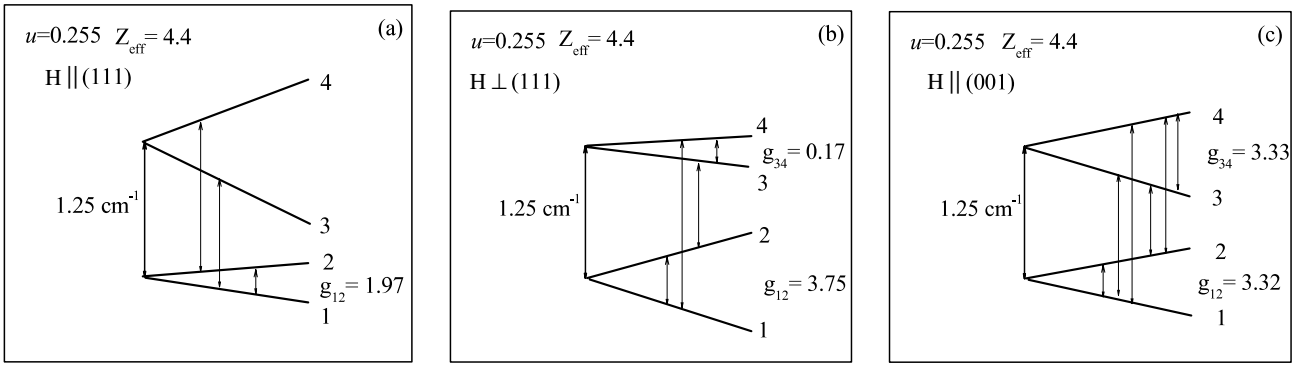

Figure 8. The splitting schemes for the Cr^{3+} ion, which is placed into the trigonal distorted octahedral crystal field created by the selenium ions: (a) $H\|(111)$; (b) $H_\perp(111)$; (c) $H\|(001)$. The arrows mark the allowed transitions: $f_1 = 9.7173$ GHz $= 0.324$ cm^{-1} and $f_2 = 34.163\,99$ GHz $= 1.1395$ cm^{-1}.

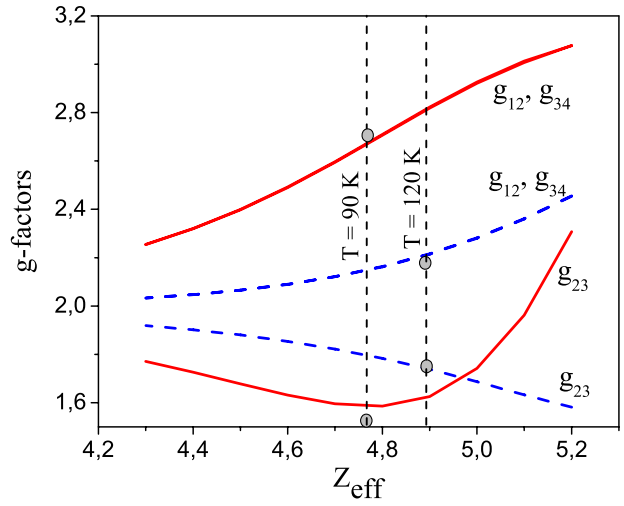

Figure 9. The dependences of the g-factor on the $Z_{\rm eff}$ for $H\|(001)$ and the low frequency quantum $f_1 = 9.7173$ GHz $= 0.324$ cm^{-1}: dashed blue lines correspond to the spinel structure with $u = 0.2505$, solid red lines—$u = 0.2510$. g-factor values correspond to the allowed transitions like $1 \leftrightarrow 2$, $3 \leftrightarrow 4$ and $2 \leftrightarrow 3$ for both structures. The circles in the figure mark experimental g-factor values, measured at 120 and 90 K (see figure 3(c)).

frequency quantum at $f_1 = 9.7173$ GHz $= 0.324$ cm^{-1} in the field $H\|(001)$ for the two spinel structures characterized by values $u = 0.2505$ and $u = 0.2510$, respectively. Due to a small discrepancy between u and u_0, the ZFS value between the lowest doublets is near 1–2 cm^{-1}, that creates the level crossing and points out its non-equidistant behavior even at low magnetic fields. It is interesting to note that g-factor values, measured at $T = 90$ K, correspond to $Z_{\rm eff} = 4.76$, while g-factor values obtained at $T = 120$ K correspond to $Z_{\rm eff} = 4.9$. This is in accordance with expectation that an increase of the trigonal distortions (parameter u) relates to an increase of the crystal field strength, i.e. to the effective nuclear charge lowering.

Thus, we have arrived with the possible scenario of the ESR fine structure development.

(1) At room temperature, the $(CrSe_6)^{9-}$ octahedral cell in the $HgCr_2Se_4$ spinel cluster can be considered as the undistorted one ($u = 0.25$). In this case, the lowest level splitting is equidistant and, hence, the ESR spectrum demonstrates a single line with isotropic g-factor which is equal to $g \approx 1.98$.

(2) With the temperature decrease the trigonal distortions develop, that results in the quartet splitting and appearance of the ZFS between two doublets. At the small ZFSs the transitions are not equivalent and are allowed both within doublets and between them. In this case, the ESR spectrum represents a set of lines with different g-factors, intensities and widths (figures 2 and 3). The development of trigonal distortion results in a decrease of the octahedron cell volume and, hence, in an increase of the crystal field strength.

5. Conclusion

Summarizing all our data, one can conclude that the $Hg_{1-x}Cr_xSe$ compound, grown by the solid state recrystallization method, contains micro-inclusions of the $HgCr_2Se_4$ spinel phase clusters. The microstructure analysis has allowed us to reveal that the spinel clusters exist starting with the lowest $x = 0.03$ chromium content and occur up to $x = 0.1$. The ESR studies demonstrate that the experimentally observed spectra possess properties which are characteristic for the spinel phase and at low temperatures they show a fine structure. Numerical investigations uncover the interconnection of the ESR fine structure with trigonal distortions of the $(CrSe_6)^{9-}$ octahedral cell, which are an inherent feature of the spinel lattice [17, 27]. The Cr^{2+} ions in the tetrahedral cell (the $(CrSe_4)^{6-}$ cluster in the host $Hg_{1-x}Cr_xSe$ selenide matrix) cannot lead to the ESR response. It is most unlikely that the origin of the ESR signal results from the strongly distorted tetrahedral $(CrSe_4)^{5-}$ cells (the Cr^{3+} ion is in the tetrahedral selenide environment). The detailed experimental study of the ESR fine structure on the u-value is of interest hereafter.

Acknowledgments

We thank V N Berzhanski and S Yu Karelin for helpful discussions. We would like to thank the ESR Division at

Bruker-BioSpin GmbH, Rheinstetten, Germany, for assistance with data collection on the ELEXSYS E580 Super Q-FT spectrometer.

References

[1] Erwin S C and Žutić I 2004 Tailoring ferromagnetic chalcopyrites *Nat. Mater.* **3** 410

[2] Mac W, Twardowski A and Demianiuk M 1996 s, p–d exchange interaction in Cr-based diluted magnetic semiconductors *Phys. Rev.* B **54** 5528

[3] Ohno H, Chiba D, Matsukura F, Omiya T, Abe E, Dietl T, Ohno Y and Ohtani K 2000 Electric-field control of ferromagnetism *Nature* **408** 944

[4] Cui X Y, Medvedeva J E, Delley B, Freeman A J, Newman N and Stampfl C 2005 Role of embedded clustering in dilute magnetic semiconductors: Cr doped GaN *Phys. Rev. Lett.* **95** 256404

[5] Edmonds K W 2007 Holes respond to strain *Nat. Mater.* **6** 472

[6] Filippetti A and Hill N A 2000 Magnetic stress as a driving force of structural distortions: the case of CrN *Phys. Rev.* B **85** 5166

[7] Erwin S C, Lee S-H and Scheffler M 2002 First-principles study of nucleation, growth, and interface structure of Fe/GaAs *Phys. Rev.* B **65** 205422

[8] Dietl T 2003 Functional ferromagnets *Nat. Mater.* **2** 646

[9] Žutić I, Fabian J and Das Sarma S 2004 Spintronics: fundamentals and applications *Rev. Mod. Phys.* **76** 323

[10] Samarth N 2007 Ferromagnetic semiconductors ruled by a magnetic-rich minority *Nat. Mater.* **6** 403

[11] Kuroda S, Nishizawa N, Takita K, Mitome M, Bando Y, Osuch K and Dietl T 2007 Origin and control of high-temperature ferromagnetismin semiconductors *Nat. Mater.* **6** 440

[12] Picozzi S 2004 Engineering ferromagnetism *Nat. Mater.* **3** 349

[13] Tsidil'kovskii I M 1992 Gapless semiconductors with magnetic admixtures which induce the resonance donor states *Sov. Phys.—Usp.* **162** 63

[14] Prozorovskii V D, Reshidova I Yu and Paranchich Yu S 1995 Electron spin resonance and magnetic susceptebility of $Hg_{1-x}Cr_xSe$ solid solution with $0.00112 \leqslant x \leqslant 0.07$ *Low Temp. Phys.* **21** 813

[15] Prozorovskii V D, Reshidova I Yu, Paranchich S Yu and Romanyuk V R 2002 Influence of Cr concentration on the structural and magnetic properties of the diluted magnetic semiconductor $Hg_{1-x}Cr_xSe$ *Low Temp. Phys.* **28** 880

[16] Sakai N and Pifer J H 1986 Effect of hydrostatic pressure on the exchange interactions in a ferromagnetic spinel $CdCr_2Se_4$ *Phys. Rev.* B **33** 1875

[17] Baltzer P K, Wojtovicz P J, Robbins M and Lopatin E 1966 Exchange interactions in ferromagnetic chromium chalcogenide spinels *Phys. Rev.* **151** 367

[18] Berzhanski V N, Gavrichkov S A and Ivanov V I 1982 Electron spin relaxation in chromium chalcogenide spinels *Sov. Phys.—Solid State* **24** 1262

[19] Berzhanski V N, Ivanov V I and Lazuta A V 1982 Magnetic field effect of the critical EPR-dynamics of the cubic ferromagnets $CdCr_2Se_4$ and $CdCr_2S_4$ *Solid. State Commun.* **44** 771

[20] Bersuker I B 1996 *Electronic Structure and Properties of Transition Metal Compounds: Introduction to the Theory* (New York: Wiley–Interscience)

[21] Abragam A and Bleaney B 1970 *Electron Paramagnetic Resonance of Transition Ions* (Oxford: Clarendon)

[22] Zhitlukhina H, Lamonova K V, Orel S M and Pashkevich Yu G 2005 Evolution of the spin state of a 3d ion in a pyramidal complex *Low Temp. Phys.* **31** 963

[23] Zhitlukhina E S, Lamonova K V, Orel S M, Lemmens P and Pashkevich Yu G 2007 Spin state transformations of a 3d ion in the pyramidal environment and under lattice distortions *J. Phys.: Condens. Matter* **119** 156216

[24] Slater J 1930 *Phys. Rev.* **36** 57

[25] Condon E U and Shortely G H 1935 *The Theory of Atomic Spectra* (New York: Cambridge University Press)

[26] Sugano S, Tanabe Y and Kamimura H 1970 *Multiplets of Transition-Metal Ions in Crystals* (New York: Academic)

[27] Francisco E and Pueyo L 1987 Accurate calculation of spin–orbit coupling constants for 3d atoms and ions with effective core potentials and reduced basis sets *Phys. Rev.* A **36** 1978

[28] Francisco E and Pueyo L 1988 Theoretical spin–orbit constants for 3d ions in crystals *Phys. Rev.* B **37** 5278

[29] Sommerfeld A and Wentzel G 1921 *Z. Phys.* **7** 86

[30] Bersuker I B 1984 *The Jahn–Teller Effect and Vibronic Interactions in Modern Chemistry* (New York: Plenum)

[31] Nagel R and Lutz H D 1996 Crystal structure of chromium mercury selenide, Cr_2HgSe_4 *Z. Kristallogr.* **211** 927

[32] Boonman M E J, Mac W, Twardowski A, Wittlin A, van Bentum P J M, Maan J C and Demianiuk M 2000 High-magnetic-field EPR of Cr-based diluted magnetic semiconductors *Phys. Rev.* B **61** 5358

[33] Shannon R D 1972 *Acta Crystallogr.* A **32** 751

[34] Göbel H 1976 Local lattice distortions in chromium chalcogenide spinels at low temperatures *J. Magn. Magn. Mater.* **3** 143